Spectroscopic and Theoretical Study of Push−Pull Chromophores Containing Thiophene-Based Quinonoid Structures as Electron Spacers

Begoña Milián,[†] Enrique Ortí,[†,*] Víctor Hernández,[‡] Juan T. López Navarrete,[‡,*] and Tetsuo Otsubo[§]

Institut de Ciència Molecular, Universitat de València, 46100-Burjassot (Valencia), Spain, Departamento de Química Física, Facultad de Ciencias, Universidad de Málaga, 29071 Málaga, Spain, and Department of Applied Chemistry, Faculty of Engineering, Hiroshima University, Kagamiyama 1-4-1, Higashi, Hiroshima 739, Japan

Received: May 27, 2003; In Final Form: September 5, 2003

Donor−acceptor chromophores containing three different types of thiophene-based electron spacers and the same donor (1,3-dithiol-2-ylidene) and acceptor (dicyanomethylene) end groups have been investigated by infrared and vis-near-IR absorption spectroscopies with the aim of elucidating the ability of the heteroquinonoid spacers as electron transmitters. Density functional theory calculations have been carried out, both within the standard and the time-dependent formalisms, to assign the most relevant electronic and infrared features of these chromophores and to assess useful information about their molecular structures. Both theoretical calculations and vibrational spectra demonstrate the occurrence of a sizable intramolecular charge transfer from the electron-donor unit to the electron-acceptor group in the ground state. The optical properties of the chromophores are strongly influenced by the electron spacer. The intense optical absorptions recorded in the visible mainly correspond to the $\pi-\pi^*$ excitation of the oligothienoquinonoid bridge. As an additional merit of these molecular materials, their infrared spectra recorded at various temperatures between −170 and +180 °C reveal, at the molecular level, their high thermal stability, what has importance for their potential use in molecular electronics and optoelectronic devices.

1. Introduction

Electrooptically active organic materials are currently being investigated for their use in photonic devices for telecommunications and optical information processing.[1] Electrooptic materials usually involve a host polymeric matrix containing second-order nonlinear optical (NLO) chromophores either as guest molecules or covalently attached to the polymer backbone. Dipolar push−pull chromophores constitute the widest class of compounds investigated for their NLO properties.[2−8] These push−pull NLO-phores are basically constituted by an electron-donor (D) and an electron-acceptor (A) group interacting through a π-conjugated spacer.

It is well recognized that the NLO activity of push−pull chromophores is determined not only by the strength of the D−A pair but also more subtly by the π-conjugated spacer.[3] When comparing typical spacers such as polyenes and oligophenylenes or oligothiophenes of the same chain length and bearing the same D−A pair, a more pronounced redshift (in a given solvent) is commonly observed for the low energy absorption maximum, λ_{max}, in polyenes than in oligophenylenes or oligothiophenes, indicative of an efficient electron transmission from the donor to the acceptor. The bathochromic dispersion of the visible absorption of the push−pull chromophore is even more intensified in high polar solvents. This positive solvatochromism has been commonly regarded as an indication of molecular nonlinearity ($\mu\beta$) of NLO-phores.[9−11] However, it was recently reported that some polyenes attached to a strong D−A pair display an inverted solvatochromism.[12,13] Their λ_{max} exhibits a redshift with an increase of solvent polarity up to a certain polarity limit and then reverses this trend with a further increase of solvent polarity beyond that limit. Clearly, such spectroscopic behavior is not a simple attribute of the D−A strength but is also associated with the electronic properties of the π-conjugated spacer.

Although polyenic systems represent in principle the most effective way to achieve charge redistribution between the donor and the acceptor end groups, and D−A polyenes have been shown to exhibit huge nonlinearities,[3] the well-known limited chemical and photothermal stability of extended polyenes might represent an obstacle to the practical applications of the derived NLO-phores. As regards oligophenylenes, the efficiency of electron transmission is limited by the large aromaticity of the benzene ring, which has a detrimental effect on the second-order polarizabilities. In comparison with oligophenylenes, oligothiophenes behave as very efficient electron relays almost comparable to polyenes,[3,14] because of the lower resonance energy of thiophene compared to benzene, and have been shown to give larger contributions to $\mu\beta(0)$.[10,15,16] Oligophenylenes attain a rapid saturation beyond the terphenyl unit, whereas oligothiophenes have a strong tendency to increase $\mu\beta(0)$ with increasing the number of thiophene units. Aside from the electron transmission efficiency, another merit of oligothiophenes is their inherent stability from which thiophene-based D−A chromophores should benefit.[17,18]

One of us has reported on the synthesis of promising NLO-phores in which the 1,3-dithiol-2-ylidene donor group and the dicyanomethylene acceptor group are linked by oligothieno-

* To whom correspondence should be addressed. E-mail: teodomiro@uma.es (J.T.L.N.); enrique.orti@uv.es (E.O.).
[†] Universitat de València.
[‡] Universidad de Málaga.
[§] Hiroshima University.

10.1021/jp0354651 CCC: $25.00
Published on Web 10/11/2003

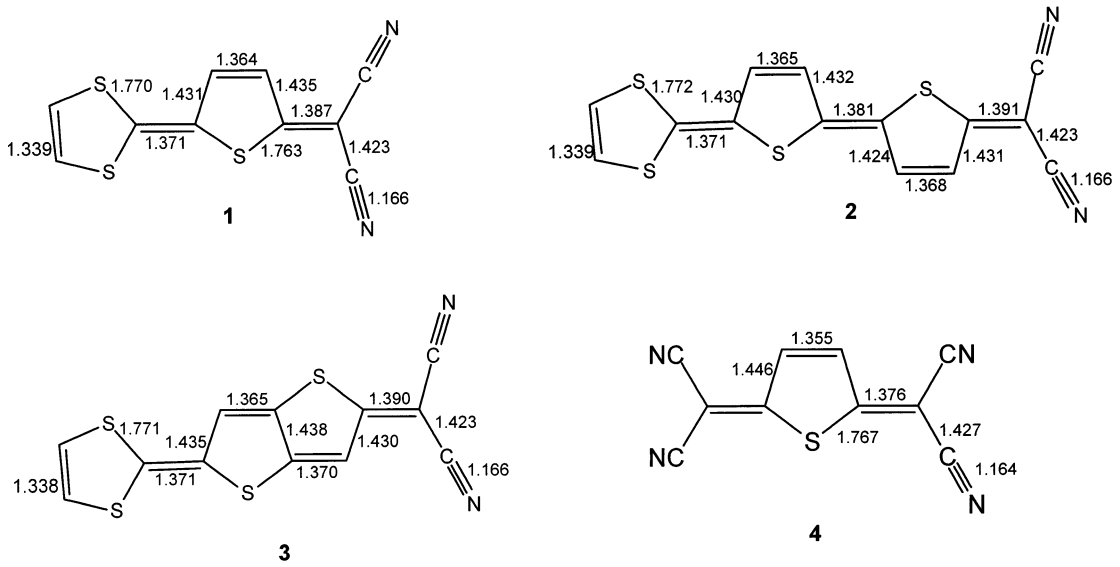

Figure 1. Selected B3LYP/6-31G** bond lengths (in Å) calculated for **1**−**3** and for thiophene-TCNQ (**4**).

quinonoid spacers (structures **1**−**3** in Figure 1).[19] As has been shown for various oligothienoquinonoid analogues of tetracyano-*p*-quinodimethane (TCNQ),[20] the use of the heteroquinonoid bridge leads to extensively polyconjugated systems which exhibit electron delocalizations comparable to those obtained in aromatic oligothiophenes. The electronic features of the bridge are however markedly different depending on the quinonoid or aromatic structure of the oligothiophene.

Since the discovery of intrinsic conducting organic polymers, vis-near-IR electronic absorption and infrared and Raman spectroscopies have been successfully used as complementary techniques to study many different types of π-conjugated oligomers and polymers. Vibrational spectroscopy is particularly useful to assess valuable information regarding (i) the degree of π-conjugation in the neutral state,[21,22] (ii) the structure and size of the electronic defects or charge carriers generated upon doping,[23] and (iii) the analysis of the intramolecular charge transfer (ICT) taking place in D−A chromophores containing π-conjugated electron spacers.[24] The effective conjugation coordinate (ECC) theory[25] has been demonstrated to provide a suitable framework for the interpretation of the unusual vibrational features of the π-conjugated systems in their neutral, doped, and photoexcited states.

Particular attention has been paid over the past few years to the theoretical analysis of the electronic and vibrational spectra within the framework of density functional theory (DFT) calculations. The successful performance of this approach for computing spectroscopic properties is at present well established.[26−29] The methodology has been shown to yield reliable predictions and interpretations of the electronic and vibrational spectra of many organic molecules.

We here describe the infrared and vis-near-IR spectra of the D−A chromophores **1**-**3** depicted in Figure 1, which contain three different quinonoid-type thiophene-based π-conjugated units as electron spacers, with the aim of gaining knowledge about the effectiveness of the electron transmission from the donor to the acceptor. The degree of intramolecular charge transfer is estimated with the help of DFT calculations, which allow for a detailed analysis of the spectral features and of the molecular structures. The thermal stability of the NLO-phores is also analyzed, at the molecular level, by recording the infrared spectra at various intermediate temperatures between −170 and +180 °C.

2. Experimental and Theoretical Details

The synthesis and purification of compounds **1**-**3** have been described elsewhere.[19] Solvents (1,2-dichloromethane, formamide, *N*,*N*-dimethylformamide, and acetonitrile) of analytical grade were purchased from Aldrich. Vis-near-IR absorption spectra were recorded on a Perkin-Elmer Lambda 19 spectrometer using freshly prepared solutions. Fourier transform infrared absorption spectra were recorded on a Bruker Equinox 55 FT-IR spectrometer. Solid samples were ground to a powder and pressed in KBr pellets. IR spectra were collected with a spectral resolution of 2 cm^{-1} and averaged over 50 scans. Interference from atmospheric water vapor was minimized by purging the instrument for 10−15 min with dry argon before data collection. A suitable variable-temperature cell Specac P/N 21525, with a pair of NaCl windows, was used to record the FT-IR spectra at different temperatures. This cell consists of a surrounding vacuum jacket (0.5 Torr), which contains a combination of a refrigerant dewar and a heating block as sample holder. The cell is equipped with a Copper-Constanton thermocouple that allows monitoring the temperature from −190 to +250 °C (83−523 K). The sample-KBr pellets were inserted into the heating block part of the dewar/cell holder assembly. The spectra were recorded after waiting for thermal equilibrium at the sample, which requires 20 min for every increment of 10 °C.

Density functional theory (DFT) calculations were carried out by means of the Gaussian 98 program package[30] running on SGI Origin 2000 computers and IBM RS/6000 workstations. All calculations were performed using the Becke's three-parameter exchange functional combined with the LYP correlation functional (B3LYP).[31] The B3LYP functional is known to yield molecular geometries similar to those afforded by MP2 calculations.[28,32] The force fields calculated with the B3LYP functional yield infrared spectra in very good agreement with the experiment.[29,33] The standard 6-31G**,[34] 6-31++G**,[35] and Dunning's aug-cc-pVDZ[36] basis sets were used in the calculations. Harmonic vibrational frequencies and infrared intensities were calculated analytically on the ground-state optimized geometries. The computed frequencies were uniformly scaled down by a factor of 0.96 as recommended by Scott and Radom.[29] This simple scaling of the vibrational force field is often accurate enough to disentangle serious experimental misassignments. All calculated vibrational frequencies reported along the paper are thus scaled values. The theoretical spectra

SCHEME 1

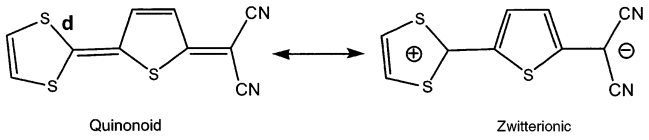

were obtained by convoluting the scaled frequencies with Gaussian functions (10 cm^{-1} width at the half-height). The relative heights of the Gaussians were determined from the infrared intensities calculated theoretically.

Vertical electronic excitation energies were computed by using the time-dependent DFT (TDDFT) approach.[37,38] Numerical applications reported so far indicate that TDDFT employing current exchange-correlation functionals performs significantly better than HF-based single excitation theories, such as the single-excitation configuration interaction (CIS) approach, for the low-lying valence excited states of both closed-shell and open-shell molecules.[26,39] In recent works, the TDDFT approach has been successfully applied to the study of the electronic spectra of aromatic,[27,40] quinonoid,[20a] and push−pull[41] oligothiophenes. TDDFT calculations were carried out using the B3LYP functional and the 6-31G** basis set on the molecular geometries previously optimized at this theoretical level. The 12 lowest-energy electronic excited states were at least computed for all of the molecules.

3. Results and Discussion

(a) Molecular Structures. The molecular geometries of compounds **1**−**3** were optimized at the B3LYP/6-31G** level assuming fully planar C_s structures. For molecule **2**, an anti arrangement of the thiophene rings was adopted. The geometry of **1** was also optimized by using the more extended Pople's 6-31++G**[35] and Dunning's aug-cc-pVDZ[36] basis sets, which include diffuse functions. Calculations showed that these functions have almost no influence on the optimized geometry, the maximum difference found for the bond lengths being of only 0.003 Å.

Figure 1 displays the optimized B3LYP/6-31G** bond lengths calculated for molecules **1**−**3**. The shortest carbon−carbon (CC) length corresponds to the C═C bond of the electron-donating dithiole ring (1.34 Å). For the three π-conjugated spacers, the thiophene $C_\alpha-C_\beta$ bonds have lengths of about 1.43 Å and the $C_\beta-C_\beta$ bonds (1.36−1.37 Å), the $C_\alpha-C_{sp^2}$ bonds connecting the spacer to the push and pull end groups (1.37 and 1.39 Å, respectively), and the inter-ring $C_\alpha-C_{\alpha'}$ bond in compound **2** (1.38 Å) have shorter lengths. These data are in good agreement with the X-ray structure reported for molecule **1**[19] and show that the ground-state equilibrium geometries of molecules **1**−**3** correspond to heteroquinonoid structures. The backbone of the oligothiophene spacer exhibits a reversal of the single-double CC bond alternation pattern with respect to that commonly observed for aromatic oligothiophenes, for which the $C_\beta-C_\beta$ bonds and the inter-ring $C_\alpha-C_{\alpha'}$ bonds are longer than the $C_\alpha-C_\beta$ bonds. As discussed below, this reversal of the structural pattern has important consequences on the vibrational and electronic properties of these novel molecular materials.

Figure 1 also shows the bond lengths calculated for the thiophene analogue of the TCNQ molecule (**4,** C_{2v} symmetry) for comparison purposes. The single−double CC bond length alternation (BLA) computed for the thiophene ring is 0.022 Å smaller for the push−pull molecule **1** (0.069 Å) than for **4** (0.091 Å), the exocyclic CC bond connecting the ring to the dicyanomethylene group being 0.011 Å longer for **1**. These differences evidence that the molecular structure of **1** has a less pronounced quinonoid character than that of **4**, thus suggesting a certain contribution from the zwitterionic resonant structure sketched in Scheme 1 to the ground state of **1**. The zwitterionic form implies an intramolecular charge transfer from the electron-donor to the electron-acceptor unit of the push−pull chromophore.

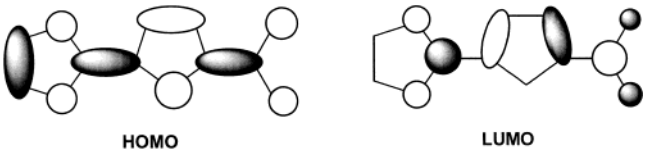

Figure 2. Electronic density contours calculated for the HOMO and the LUMO of molecule **1**.

The geometries optimized for molecules **2** and **3** show that the oligothiophene bridge presents slightly different structures near the end-capping groups. For both molecules, the thiophene ring closer to the $C(CN)_2$ group exhibits a smaller BLA value than the thiophene ring near the dithiole unit, and the C═C bond connecting the electron spacer to the donor group is 0.02 Å shorter than that linking the spacer to the electron-acceptor group. These results indicate the occurrence of some intramolecular charge transfer, which partially aromatizes the molecular environment of the electron-acceptor group. A similar behavior was previously found for a series of second-order NLO-phores built up around a central aromatic oligothiophene spacer.[24]

The net atomic charges calculated using Mulliken population analysis support the contribution of the zwitterionic form to the molecular structure of compounds **1**−**3**. The charge accumulated by the dicyanomethylene unit is similar for the three compounds (**1**: −0.34*e*; **2**: −0.36*e*; **3**: −0.35*e*) and doubles that borne by each $C(CN)_2$ group in compound **4** (−0.18e).

(b) Intramolecular Charge Transfer. A structural approach based on the values obtained for the optimized bond distances was used to estimate the degree of charge transfer from the donor group to the acceptor unit in molecules **1**-**3**. The dithiole C−S bonds adjacent to the exocyclic double bond (bonds *d* in Scheme 1) were chosen to measure the charge transfer, because they are largely affected by the effective charge on the dithiole moiety. As depicted in Figure 2, the highest occupied molecular orbital (HOMO) is π-antibonding with respect to the C−S *d* bonds. An increase of the positive charge on the dithiole ring lowers the electron density and causes a sizable shortening of the *d* bonds. Such reasoning has been previously used in the determination of the degree of ionicity of tetrathiafulvalene (TTF) and its derivatives in charge-transfer complexes[42] and is employed here to estimate the intramolecular charge transfer.

Figure 3 correlates the B3LYP/6-31G** lengths calculated for the C−S *d* bonds of TTF in its neutral (1.7877 Å), radical cation (1.7475 Å), and dication (1.7135 Å) states with the net charge (δ^+) borne by each dithiole ring ($\delta^+ = 0e$, $+0.5e$, and $+1.0e$, respectively). To have a higher number of points to perform the correlation, a symmetric D_{2h} π-dimer of TTF with global charges of $+1e$ and $+3e$ was optimized, so that net charges of $+0.25e$ and $+0.75e$ per dithiole ring were obtained. The excellent linear correlation found between the C−S *d* distances and the dithiole charges allows the degree of charge transfer that takes place in **1** (d = 1.7675 Å, $\delta^+ = +0.25e$), **2** (d = 1.7694 Å, $\delta^+ = +0.23e$), and **3** (d = 1.7691 Å, $\delta^+ = +0.23e$) to be estimated.[43] The values obtained for δ^+ indicate a certain degree of intramolecular charge transfer between the donor and the acceptor units, which slightly decreases with the size of the oligothiophene bridge.

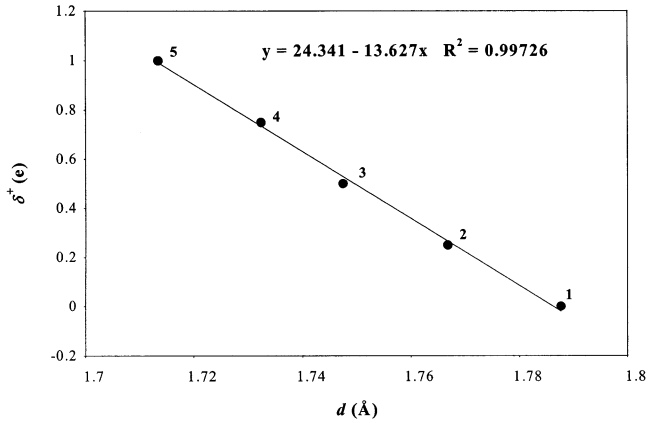

Figure 3. Correlation between the length of the C−S *d* bonds (B3LYP/6-31G** values) and the charge borne by each dithiole ring for five different oxidation states of TTF [1, $(TTF)^0$; 2, $(TTF)_2^+$; 3, $(TTF)^+$; 4, $(TTF)_2^{+3}$; 5, $(TTF)^{+2}$].

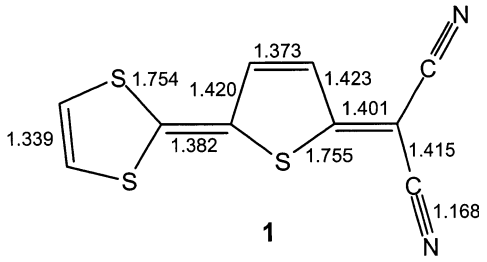

Figure 4. Selected B3LYP/6-31G** bond lengths (in Å) calculated for **1** in the presence of water.

TABLE 1: B3LYP/6-31G Values Calculated for the Dipole Moment μ, the C−S *d* Bond Distance[a], and the Charge Transfer δ^+ of Molecule 1 in Different Solvents**

solvent	μ (D)	*d* (Å)	δ^+(e)
gas phase	11.8	1.7675	+0.25
dichloromethane	16.1	1.7571	+0.40
acetone	16.6	1.7562	+0.41
dimethyl sulfoxide	16.8	1.7552	+0.42
water	18.6	1.7525	+0.46

[a] The value of *d* is obtained as the average of the lengths calculated for the two C−S dithiole bonds adjacent to the exocyclic C=C bond.

The degree of intramolecular charge transfer was also calculated in solution, because the polarity of the solvent helps in stabilizing the charge-separated zwitterionic form. The geometry of **1** was thereby reoptimized in the presence of dichloromethane (ϵ = 8.93), acetone (ϵ = 20.7), dimethyl sulfoxide (ϵ = 46.7), and water (ϵ = 78.39) making use of the polarized continuum model (PCM). This model considers the solvent as a continuous medium with a dielectric constant ϵ, and the solute is represented by means of a cavity built with a number of interlaced atomic spheres.[44] The optimized bond lengths calculated in water for **1** are given in Figure 4 as an example of the influence of the solvent polarity.

As expected, the degree of charge transfer increases with the polarity of the solvent. The Mulliken population analysis shows that, in polar media, the positive charge on the dithiole ring and the negative charge on the $C(CN)_2$ group increase, whereas the charge borne by the central thiophene ring remains nearly constant. The molecular dipole moment (μ) thus increases from 11.8 D, for the isolated molecule in vacuum, to 18.6 D in water (see Table 1). Using the linear correlation of Figure 3 and the values of the C−S *d* bond distances summarized in Table 1, charge transfers of 0.40*e* (dichloromethane), 0.41*e* (acetone), 0.42*e* (dimethyl sulfoxide), and 0.46*e* (water) are predicted. These values are significantly higher than that obtained in the gas phase (0.25*e*) and indicate that, in polar media, the zwitterionic form depicted in Scheme 1 has a larger contribution to the molecular structure. As a consequence, a lower BLA value is predicted for the conjugated spacer of **1** in water than in the gas-phase (cf. Figures 1 and 4), consistent with a reduction of the heteroquinonoid character of the molecule in solution.

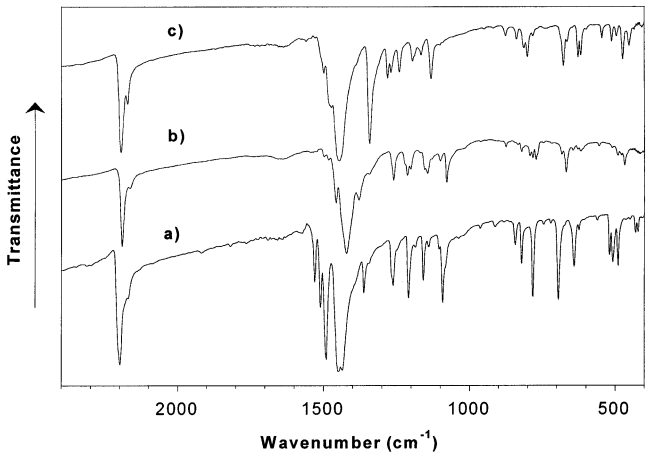

Figure 5. Fourier transform infrared spectra of (a) **1**, (b) **2**, and (c) **3** over probe energies of 2400−400 cm^{-1}.

(c) Vibrational Properties. The Fourier transform infrared spectra recorded for solid samples of **1**−**3** in the 2400−400 cm^{-1} region are shown in Figure 5 (Raman spectra are available upon request to the authors). The complete assignment of the vibrational spectra of these push−pull chromophores to particular vibrations is beyond the scope of our analysis. We will restrict our discussion to the more relevant observations of general validity for the class of push−pull chromophores:

(1) The IR (and the Raman) spectra display much more bands than for the neutral forms of symmetrically end-capped α,α′-oligothiophenes due, among other factors, to the lowering of molecular symmetry.[22]

(2) The IR absorptions recorded for push−pull oligothiophene chromophores are stronger than those observed for nonpolar oligothiophenes due to the large dipole moment changes induced by the molecular vibrations, particularly for the bands appearing in the 1600−1400 cm^{-1}. This is quite evident for **2** and **3**, for which the relative intensities of the ν(C=C) stretching vibrations of the π-conjugated skeleton are stronger than the remainder infrared vibrations.

(3) The IR and Raman spectra of a given push−pull chromophore show many similarities, both in the peak positions and in the relative intensities of the different vibrational features. This is not the case for nonpolar oligothiophenes (either symmetrically or asymmetrically substituted), for which the IR and Raman spectra are complementary: the strongest IR absorptions display a weak or negligible Raman-activity, and vice versa. The Raman spectra of aromatic nonpolar oligothiophenes show very few lines with an overwhelming intensity, because of the strong polarizability changes of the π-conjugated backbone along particular totally symmetric skeletal vibrations, termed as collective ECC modes.[25] In the case of push−pull chromophores, these ECC modes are also strongly activated in the infrared because of the strong polarization of the molecular backbone induced by the attachment of polar end groups, so that the initially IR-silent totally symmetric ECC modes also give rise to large charge fluxes along the conjugated C=C/C−C path, thus gaining a strong IR-activity.

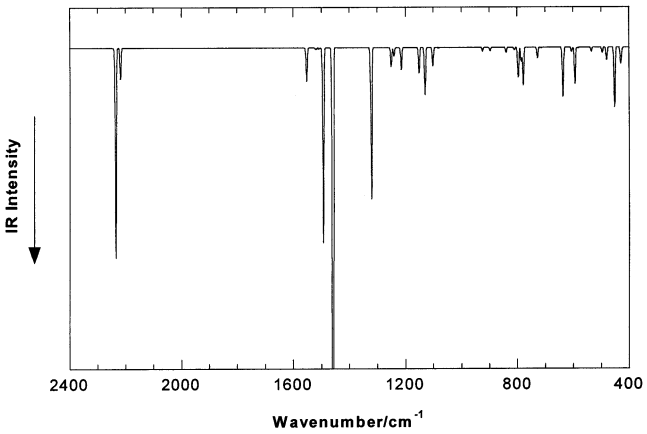

Figure 6. B3LYP/6-31G** infrared spectrum calculated for **3** over probe energies of 2400−400 cm^{-1}.

TABLE 2: Vibrational Infrared Frequencies (in cm^{-1}) Measured and Calculated for the ν(C≡N) Band[a]

compound	exp.	B3LYP/6-31G**
1	2201 (2172)	2238 (2221)
2	2192 (2165)	2235 (2216)
3	2196 (2173)	2236 (2219)
4	2222[b]	2251

[a] The frequency of the shoulder is given within parentheses. [b] Data from ref 47.

The IR spectra of **1**−**3** show a similar profile with differences in the relative intensities of the observed bands, particularly in the low-energy region. Three main spectral ranges can be distinguished in the spectra: ∼2200, 1600−1000, and 900−400 cm^{-1}. The theoretical IR spectra, calculated at the B3LYP/6-31G** level on the optimized geometries depicted in Figure 1, nicely reproduce the experimental features. As a representative example, Figure 6 plots the theoretical spectrum obtained for **3**. Nevertheless, when experimental spectra recorded on solid samples are compared with theoretical data evaluated on isolated entities, one must be cautious because solid-state intermolecular interactions can influence the relative intensities of the vibrational bands and provoke splittings of specific bands into structured peaks. In such cases, correlation between experiment and theory is not always straightforward.

The C≡N stretching vibration, ν(C≡N), is observed for the three push−pull chromophores **1**-**3** as a sharp and strong absorption at ∼2200 cm^{-1} with a second component on its low-energy side. Table 2 summarizes the wavenumbers measured for the two bands, together with the calculated values. Theory predicts the two-peak structure of the band and assigns the strongest component to a normal mode in which the two CN bonds vibrate in phase, the second absorption at ∼2170 cm^{-1} corresponding to the related out-of-phase motion.

The frequency of the ν(C≡N) band is highly sensitive to the electron density borne by the nitrile groups and downshifts either upon complexation with electron donors or upon reduction due to the lengthening of the C≡N bonds.[45,46] Taking molecule **4** as a reference, for which the ν(C≡N) band is observed as a single peak at 2222 cm^{-1},[47] the corresponding ν(C≡N) absorptions appear at significantly lower frequencies for the push−pull systems **1**−**3** and downshift along the series **1** (2201 cm^{-1}) > **3** (2196 cm^{-1}) > **2** (2192 cm^{-1}). The experimental frequencies support the occurrence of an intramolecular charge transfer toward the electron withdrawing $C(CN)_2$ group in **1**−**3** and suggest that the degree of charge transfer increases with the molecular size. Because we are analyzing a series of chromophores with the same D/A pair, this trend shows that the π-conjugated spacer also contributes to the electron density transferred to the $C(CN)_2$ group. B3LYP/6-31G** results correctly predict the experimental trend observed for the ν(C≡N) frequencies, although they underestimate the frequency changes on going from **4** to **1, 2,** and **3** (see Table 2). This result can be attributed to an underestimation of the degree of charge transfer by the theoretical calculations, but it can also be an indication of the nonnegligible influence that the intermolecular interactions taking place in the solid have on the ν(C≡N) frequencies.

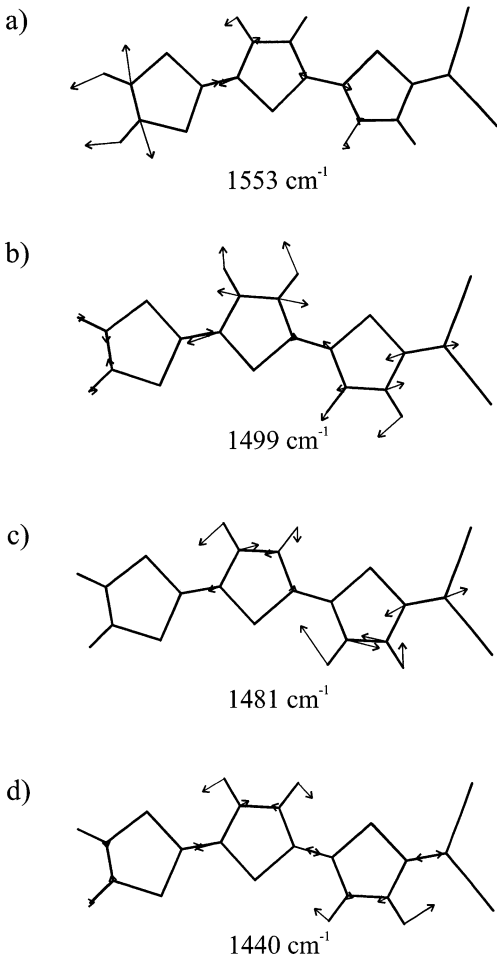

Figure 7. Schematic eigenvectors calculated at the B3LYP/6-31G** level for selected C=C stretching vibrations of molecule **2**. Scaled frequencies are given.

The infrared spectra over the range 1600−1000 cm^{-1} give us structural information about the π-conjugated oligothiophene spacer. The three molecules **1**−**3** show a broad and strong feature centered around 1450 cm^{-1}. The strongest absorptions are measured at 1452−1438 cm^{-1} for **1** (double peak), 1421 cm^{-1} for **2**, and 1447 cm^{-1} for **3**. B3LYP/6-31G** calculations predict the most intense IR-active vibration at 1465 (**1**), 1440 (**2**), and 1459 cm^{-1} (**3**) in good agreement with the experimental values. As sketched in Figure 7d for molecule **2**, this vibration corresponds to a C=C stretching mode, ν(C=C), in which all of the C=C bonds of the π-conjugated path vibrate in phase. This ν(C=C) mode is coupled with the in-plane bending of the C−H bonds of the thienyl rings. The peak position of this characteristic vibration depends on the extension of the CC π-conjugated pathway defined by the oligothiophene bridge; as the path lengthens, a more effective π-delocalization takes place, and the vibration shifts downward because of the

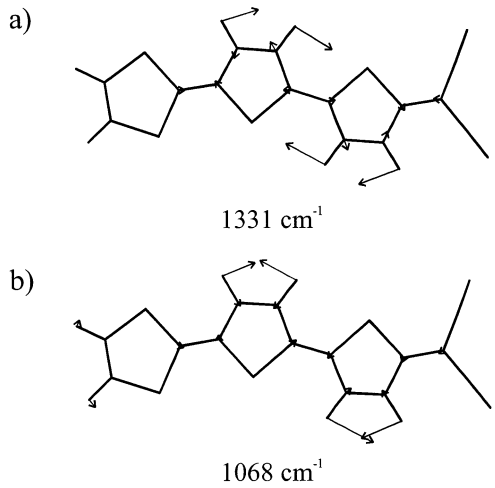

Figure 8. Schematic eigenvectors calculated at the B3LYP/6-31G** level for selected vibrations of molecule **2**. Scaled frequencies are given.

softening of the C═C double bonds.[21−25] Thus, this infrared absorption redshifts by 31 cm^{-1} from compound **1** (1452 cm^{-1}), with three conjugated double bonds, to **2** (1421 cm^{-1}), with five conjugated double bonds. This specific normal mode, which for nonpolar π-conjugated systems displays the strongest Raman-activity while being infrared-silent, acts as the primary funnel between the neutral and the zwitterionic extreme resonant canonical structures, and shows the largest[48,49] and fastest[50] nuclear displacements (and hence the largest charge fluxes) in comparison to all other IR-active normal modes.

All the peaks observed on the high-energy side of the above vibration are due to ν(C═C) stretching modes. Molecule **1** exhibits three strong and sharp infrared bands at 1531, 1511, and 1492 cm^{-1}, which are attributed to the vibrations calculated at 1551, 1519, and 1506 cm^{-1}, respectively. Their associated vibrational eigenvectors are analogous to those depicted in Figure 7a−c for molecule **2**, which also displays three well-resolved peaks above the strongest IR band at 1421 cm^{-1} but with lower relative intensities. The same modes are also IR-active for molecule **3**, the highest frequency vibration being due, for the three molecules, to the stretching of the dithiole C═C bond coupled out-of-phase with the closest exocyclic C═C bond (see Figure 7a).

Molecules **1** and **2** show medium-intensity absorption bands at 1363 cm^{-1} (calculated at 1342 cm^{-1}) and at 1379 and 1344 cm^{-1} (calculated at 1362 and 1331 cm^{-1}), respectively, due to in-plane δ(C−H) bendings. The eigenvectors associated to these vibrations are similar to that sketched in Figure 8a for **2**. The strong absorption recorded for molecule **3** at 1343 cm^{-1} (calculated at 1322 cm^{-1}) is also due to an in-plane δ(C−H) bending of the thienyl C−H bonds, although strongly mixed with the stretching of the central $C_\alpha-C_\beta$ bond tailoring the two fused thienyl rings.

The infrared fingerprint of molecules **1**−**3** in the 1300−1000 cm^{-1} spectral region is characterized by the appearance of six/seven sharp absorptions of medium intensity. Calculations correctly predict the number of experimentally recorded IR-active modes in this region, although fail somewhat in reproducing their relative intensities (cf. Figures 5c and 6). Most of these vibrations are mainly located on the electron spacer and are due to mixings of in-plane δ(C−H) bendings and stretchings of the CC single bonds. The high-frequency bands recorded at 1263 (**1**) and 1259 cm^{-1} (**2**) show also a significant contribution of the ν(C−CN) stretchings, whereas the low-frequency bands at 1093 (**1**) and 1079 cm^{-1} (**2**) are due to the pure symmetric in-phase, in-plane δ(C−H) bending of the thienyl rings (see Figure 8b). The corresponding mode appears at higher frequencies for **3** (1132 cm^{-1}) due to the coupling with the stretching of the central $C_\alpha-C_\beta$ bond.

Below 1000 cm^{-1}, molecules **1**−**3** present many weak-medium absorption bands. The bands measured at 846 and 822 cm^{-1} (**1**) and at 875 and 822 cm^{-1} (**2**) are due to C−S stretching modes. The band at higher energies mainly involves the oscillation of the thienyl C−S bonds and is predicted to shift upward with increasing the molecular size (**1**, 801 cm^{-1}; **2**, 840 cm^{-1}) in agreement with experiment. The band at lower energies is due to the antisymmetric stretching of the dithiole C−S bonds and is calculated at ∼785 cm^{-1} for both molecules. Theoretical frequencies are underestimated by ∼40 cm^{-1} because the B3LYP functional is known to overestimate the length of the C−S bonds.[51] The out-of-plane γ(C−H) bending modes, either of the thienyl or of the dithiole units (i.e., 783 and 700 cm^{-1} for **1**; 783, 771, and 668 cm^{-1} for **2**; and 801 and 677 cm^{-1} for **3**), display rather low relative intensities as compared with nonpolar oligothiophenes, for which they are usually found to give rise to the strongest IR absorptions.[22,23,25] For push−pull π-conjugated systems, the skeletal CC stretchings display by far the largest IR intensities.[24] The in-plane δ_{ring} bendings appearing below 700 cm^{-1} (i.e., 642, 624, 508, and 490 cm^{-1} for **1**; 668, 618, 490, and 467 cm^{-1} for **2**; and 627−618, 495, 474, and 452 cm^{-1} for **3**) and the out-of-plane γ_{ring} folding modes (i.e., 562 and 521 cm^{-1} for **1**; 554 and 510 cm^{-1} for **2**; and 545 and 512 cm^{-1} for **3**) are correctly predicted by calculations, but provide minor information regarding the degree of intramolecular charge transfer.

Before concluding this section, it is useful to compare the IR spectrum of molecule **2** with that previously reported for 5,5′-bis(dicyanomethylene)-5,5′-dihydro-Δ2,2′-bithiophene (**5**),[20b] a bithienoquinonoid analogue of **2**, although symmetrically capped with two electron-withdrawing $C(CN)_2$ groups. The attachment of the dithiole ring renders a more complex vibrational spectrum as the consequence of two main effects. First, the symmetry lowers from C_{2h} in **5** to C_s in **2**. More normal modes are thus expected to be activated both in the infrared and in the Raman spectra. Second, the D−spacer−A structure of the molecule induces a large permanent molecular dipole moment directed from the dithiole donor unit toward the $C(CN)_2$ acceptor group (15.6 D at the B3LYP/6-31G** level). Large charge fluxes thus take place along several molecular vibrations, significantly enhancing their IR intensities.

For molecule **5**, the strongest IR bands are observed as a doublet at 1528−1499 cm^{-1} (calculated at 1529−1493 cm^{-1}), which correspond to the antisymmetric stretchings of the C_β═C_β and the C_α═C_{sp^2} bonds, respectively.[20b] For **2**, these two modes display a very weak intensity, and it is a totally in-phase C═C stretching mode spreading over the whole π-conjugated backbone (Figure 7d), measured at 1421 cm^{-1} and calculated at 1440 cm^{-1}, which bears most of the infrared intensity. The corresponding vibration is computed at 1466 cm^{-1} for **5,** but it is not IR-active due to its totally symmetric character. The downshift of 26 cm^{-1} calculated in passing from **5** to **2** is a measure of the intramolecular charge-transfer taking place in **2,** which induces a softening of the C═C bonds due to the role played by the zwitterionic canonical structure in the stabilization of the electronic ground state.

(d) Electronic Spectra. The electronic absorption spectra of molecules **1**−**3** were recorded in a variety of solvents with different polarities (i.e., chloroform, tetrahydrofuran, 1,2-dichloro-

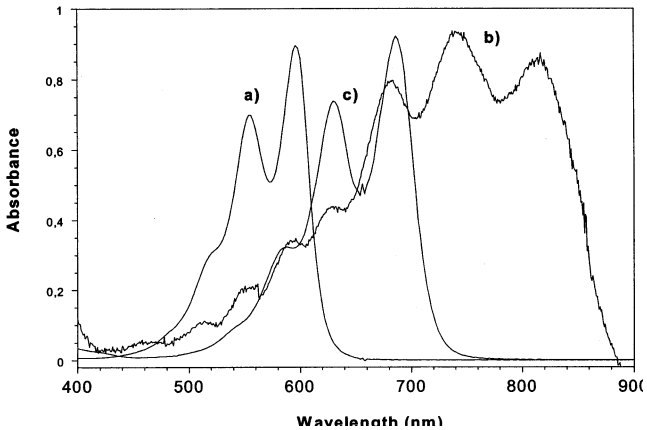

Figure 9. Vis-near-IR spectra recorded in dimethylformamide solution for **1** (a) and **2** (b) and in acetonitrile solution for **3** (c).

methane, acetonitrile, *N*,*N*-dimethylformamide, and formamide). Figure 9 displays the spectra in dimethylformamide (**1** and **3**) and acetonitrile (**2**). The three molecules show a very strong and broad electronic absorption in the visible, with a well-resolved peak structure. The maximum absorption is measured at 549 nm for molecule **1** in THF, and, as expected, it largely redshifts as the number of double bonds in the π-conjugated electron spacer increases (625 nm for **3** and 739 nm for **2**, in THF). These maximum absorption wavelengths are significantly longer than those found for aromatic bithiophene and terthiophene molecules around 300 and 350 nm, respectively.[52,53] The absorption edge for molecule **2** actually extends into the near-infrared region up to 900 nm. The absorption maxima undergo a small positive solvatochromism with increasing the polarity of the solvent. The two maxima observed for molecule **1** (see Figure 9) shift from 546 and 587 nm in chloroform to 558 and 598 nm in dimethylformamide and formamide.

It is useful to compare the electronic spectra of molecules **2** and **5**, which bear the same bithienoquinonoid spacer separating the end-capping groups. Molecule **5** also exhibits a strong and broad absorption in the visible with a maximum at 550 nm and the absorption edge around 600 nm.[47] These values are significantly blue-shifted with respect to those recorded for **2** and illustrate the bathochromic effect that the attachment of the dithiole group induces on the main optical absorption.

To investigate the nature of the electronic transitions that give rise to the absorption bands observed experimentally, the lowest-energy electronic excited states of molecules **1**−**3** were calculated at the B3LYP/6-31G** level using the TDDFT approach and the optimized geometries depicted in Figure 1. The excited states of **1** were also calculated with the more extended aug-cc-pVDZ basis set. The results derived from both basis sets are nearly the same, the maximum difference being of 0.15 eV. Table 3 collects the vertical excitation energies calculated for **1**−**3**.

Theoretical calculations predict the appearance of only one intense electronic transition in the visible region (see Table 3). The transition corresponds to the excitation to the first excited electronic state ($2^1A'$) and is computed at 2.82 eV for **1** (with a oscillator strength, *f*, of 0.76), at 2.24 eV for **2** ($f = 1.28$), and at 2.58 eV for **3** ($f = 1.15$). All of the remaining transitions calculated below 4.0 eV have small oscillator strengths ($f < 0.1$). The intense absorptions observed in the visible for **1** (549 nm, 2.26 eV), **2** (739 nm, 1.68 eV), and **3** (625 nm, 1.98 eV) are therefore assigned to $1^1A' \rightarrow 2^1A'$ electronic transitions, and their peak-structures are attributed to vibrational

TABLE 3: B3LYP/6-31G Vertical Excitation Energies (ΔE, in eV) and Oscillator Strengths (*f*) Calculated for the Singlet Electronic Excited States**

molecule	state[a]	ΔE	*f*
1	$2^1A'$	2.82	0.755
	$3^1A'$	3.86	0.005
	$4^1A'$	4.04	0.013
	$5^1A'$	4.32	0.086
	$6^1A'$	4.92	0.028
2	$2^1A'$	2.24	1.279
	$3^1A'$	2.96	0.004
	$4^1A'$	3.61	0.005
	$5^1A'$	3.73	0.025
	$6^1A'$	3.87	0.092
3	$2^1A'$	2.58	1.154
	$3^1A'$	3.23	0.006
	$4^1A'$	3.58	0.034
	$5^1A'$	3.82	0.014
	$6^1A'$	4.37	0.021

[a] Transitions to the $^1A''$ excited states are polarized perpendicularly to the molecular plane and have negligible oscillator strengths ($f < 0.0001$).

components. The energy separation between these components (1250−1350 cm^{-1}) suggests that they correspond to progressions on the totally in-phase ν(C=C) stretching mode of the conjugation path, whose frequency is expected to decrease in the excited state. B3LYP/6-31G** excitation energies overestimate the experimental values by ~0.6 eV, but nicely reproduce the redshift measured in passing from **1** to **3** (0.28 eV) and to **2** (0.58 eV). The overestimation of the lowest excitation energy by TDDFT calculations has already been reported for sulfur-containing compounds such as tetrathiafulvalene[54,55] and other conjugated and aromatic systems.[56]

For the three molecules, the $1^1A' \rightarrow 2^1A'$ transition implies a one-electron promotion from the HOMO to the LUMO. As sketched in Figure 2 for molecule **1**, the two orbitals are of π nature and spread over the whole molecule. This contrasts with what is commonly found for push−pull systems, for which the HOMO is mainly located over the donor part of the molecule while the LUMO mostly lies on the acceptor part. The different electron distribution obtained for compounds **1**−**3** is due to the quinonoid structure of the oligothiophene bridge, which determines the atomic orbital composition of the HOMO and the LUMO. The topologies of these orbitals are actually very similar to those calculated for the bithienoquinonoid molecule **5**, which only bears electron-accepting groups. The $1^1A' \rightarrow 2^1A'$ excitation for chromophores **1**−**3** therefore corresponds to a $\pi \rightarrow \pi^*$ transition, in which the oligothienoquinonoid spacer plays the main role. The nature of the electronic excitation is therefore different from that observed for the low-energy intramolecular charge transfer bands usually recorded for push−pull systems, in which a significant electron density transfer takes place from the electron-donating to the electron-accepting group. The electronic nature predicted for the absorption bands of **1**−**3** is supported by the small bathochromic effect observed for these bands when increasing the polarity of the solvent (see Figure 9).

To get more information about the charge-transfer associated with the $1^1A' \rightarrow 2^1A'$ excitation, the electron density distribution of the first excited state $2^1A'$ was characterized in vacuum. The molecular dipole moments of the three chromophores are calculated to increase by 2−3 D in passing from the ground state (**1**, 11.8 D; **2**, 15.6 D; **3**, 14.2 D) to the excited $2^1A'$ state (**1**, 14.9 D; **2**, 17.4 D; **3**, 16.8 D). This theoretical result evidences that a certain degree of charge transfer takes place along with the $1^1A' \rightarrow 2^1A'$ excitation. The interaction with

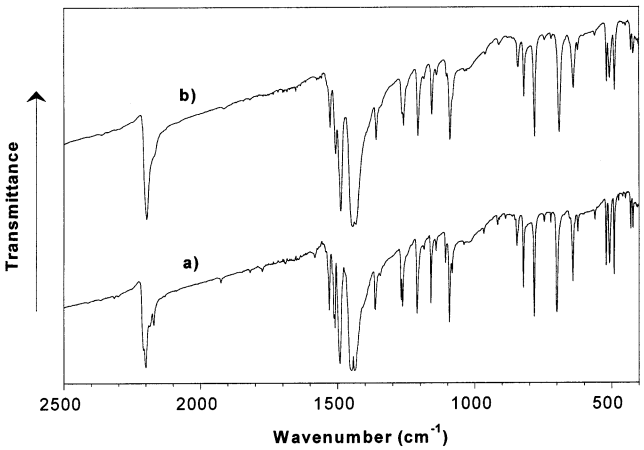

Figure 10. Thermal evolution of the FT-IR spectrum of **1** over probe energies of 2500−400 cm^{-1} measured at (a) −170 °C and (b) +180 °C.

the solvent would preferentially stabilize the $2^1A'$ state (i.e., that for which the molecular dipole moment is larger) with respect to the ground state and would determine a continuous redshift of the $1^1A' \rightarrow 2^1A'$ transition as the solvent becomes more polar. This result explains the moderate bathochromic shift observed for **1**−**3** with increasing the solvent polarity.

(e) Thermal Dependence of the Infrared Spectra. The FT-IR spectra recorded for **1** at −170 and +180 °C are shown in Figure 10 as an illustrative example of the thermal behavior of the vibrational properties of the chromophores **1**−**3**. Intermediate temperatures of −135, +20, +60, and +120 °C, were also analyzed. The melting points of the compounds were not reached in any case.

No dramatic spectral change is noticed before the maximum temperature is reached, and the spectra reversibly recover their full profiles over the whole temperature range analyzed. On raising the temperature, we observe that the infrared absorptions do not become substantially broader than the sharp and well-structured features recorded at low temperatures. This means that the internal rotation is highly hindered for this class of molecules and that solid-state intermolecular packing forces are significant even at high temperatures (causing a close molecular packing and a negligible molecular disorder). This thermal spectroscopic study also reveals that the materials can be used as active components of NLO-devices, which should be thermally stable at continuous working temperatures up to +80 °C.

4. Conclusions

The push−pull chromophores **1**−**3** bearing thiophene-based spacers end-capped with 1,3-dithiol-2-ylidene and dicyanomethylene groups have been investigated by using infrared and vis-near-IR spectroscopies together with DFT theoretical calculations. The vibrational and electronic properties of these compounds have been shown to be largely influenced by the quinonoid structure of the bridge.

The equilibrium geometries calculated for **1**−**3** evidence the occurrence of a sizable electron density transfer from the electron-donor dithiole ring to the electron-acceptor dicyanomethylene group in the ground state. The degree of charge-transfer between the donor and the acceptor units have been estimated by correlating the theoretical lengths calculated for the C−S *d* bonds of the dithiole ring and the charge borne by this ring in TTF in different oxidation states (Figure 3). A similar charge-transfer of about 0.25*e* is predicted for isolated molecules of compounds **1**−**3**. In the presence of the solvent, the degree of charge-transfer increases with the polarity of the solvent and the equilibrium geometry is intermediate between a neutral quinonoid structure and a charge-separated (zwitterionic) aromatic structure.

The IR spectra of **1**−**3** show similar profiles and have been analyzed on the basis of theoretical calculations. The spectra present many more bands than for nonpolar oligothiophenes (either symmetrically or asymmetrically substituted) because of the lowering of the molecular symmetry and the strong polarization of the molecular backbone induced by the attachment of polar end groups. The strongest absorption actually corresponds to the ν(C═C) stretching mode in which all of the C═C bonds of the π-conjugated path vibrate in phase. This mode, that is infrared-silent for nonpolar π-conjugated systems, acts as the primary funnel between the neutral and the zwitterionic resonant structures, i.e., as a funnel for the charge-transfer between the donor and the acceptor groups. The intramolecular charge transfer is corroborated by the low frequencies measured for the ν(C≡N) vibrations.

Molecules **1**−**3** exhibit a very intense and broad low-energy absorption in the electronic spectrum. The absorption is assigned to the HOMO → LUMO electronic transition and does not correspond to the typical intramolecular charge transfer band usually observed for push−pull systems. Unlike most push−pull systems, the HOMO and the LUMO of **1**−**3** spread over the whole conjugated backbone and their topologies are not dominated by the polar end groups. Thus, the HOMO → LUMO transition mainly corresponds to the $\pi \rightarrow \pi^*$ excitation of the conjugated spacer and implies only a small electron density transfer from the dithiole ring to the $C(CN)_2$ group. The optical properties of molecules **1**−**3** are therefore strongly influenced by the quinonoid structure of the electron spacer.

Acknowledgment. The research at the Universities of Valencia and Málaga was supported by the Ministerio de Ciencia y Tecnología (MCyT) of Spain through the projects PB98-1447, BQU2003-05111, BQU2003-03194, and BQU2000-1156. B.M. is grateful to the Ministerio de Educación, Cultura y Deporte of Spain for a doctoral grant.

References and Notes

(1) Prasad, P. N.; Williams, D. J. *Introduction to Nonlinear Optical Effects in Molecules and Polymers*; Wiley: New York, 1991. Zyss, J. *Molecular Nonlinear Optics: Materials, Physics and Devices*; Academic Press: Boston, 1993. Kanis, D. R.; Ratner, M. A.; Marks, T. J. *Chem. Rev.* **1994**, *94*, 195. Marder, S. R.; Perry, J. W. *Adv. Mater*. **1993**, *5*, 804. Marks, T. J.; Ratner, M. A. *Angew. Chem., Int. Ed. Engl.* **1995**, *34*, 155. Dalton, L. R.; Harper, A. W.; Ghosn, R.; Steier, W. H.; Ziari, M.; Fetterman, H.; Shi, Y.; Mustacich, R. V.; Jen, A. K.-Y.; Shea, K. J. *Chem. Mater*. **1995**, *7*, 1060. Shi, Y.; Zhang, C.; Bechtel, J. H.; Dalton, L. R.; Robinson, B. H.; Steier, W. H. *Science* **2000**, *288*, 119.

(2) Wolf, J.; Wortmann, R. *Adv. Phys. Org. Chem.* **1999**, *32*, 121. Long, N. J. *Angew. Chem., Int. Ed. Engl*. **1995**, *34*, 21.

(3) Marder, S. R.; Gorman, C. B.; Tiemann, B. G.; Cheng, L. T. *J. Am. Chem. Soc*. **1993**, *115*, 3006. Marder, S. R.; Cheng, L. T.; Tiemann, B. G. *J. Chem. Soc., Chem. Commun*. **1992**, 672. Marder, S. R.; Cheng, L. T.; Tiemann, B. G.; Friedli, A. C.; Blanchard-Desce, M.; Perry, J. W.; Skindhoj, J. *Science* **1994**, *263*, 511.

(4) Mignani, G.; Leising, F.; Meyreux, R.; Samson, H. *Tetrahedron Lett*. **1990**, *31*, 4743. Jen, A. K.-Y.; Rao, V. P.; Drost, K. J.; Wong, K. Y.; Cava, M. P. *J. Chem. Soc., Chem. Commun*. **1994**, 2057. Rao, V. P.; Cai, Y. M.; Jen, A. K.-Y. *J. Chem. Soc., Chem. Commun*. **1994**, 1689.

(5) Rao, V. P.; Jen, A. K.-Y.; Wong, K. Y.; Drost, K. J. *J. Chem. Soc., Chem. Commun*. **1993**, 1118. Gilmour, S.; Montgomery, R. A.; Marder, S. R.; Cheng, L.-T.; Jen, A. K.-Y.; Cai, Y.; Perry, J. W.; Dalton, L. R. *Chem. Mater*. **1994**, *6*, 1603. Boldt, P.; Bourhill, G.; Bräuchle, C.; Jim, Y.; Kammler, R.; Müller, C.; Rase, J.; Wichern, J. *Chem. Commun*. **1996**, 793. Wu, X.; Wu, J.; Liu, Y.; Jen, A. K.-Y. *J. Am. Chem. Soc*. **1999**, *121*, 472. Wu, X.; Wu, J.; Liu, Y.; Jen, A. K.-Y. *Chem. Commun*. **1999**, 2391.

(6) Sun, S.-S.; Zhang, C.; Dalton, L. R.; Garner, S. M.; Chen, A.; Steier, W. H. *Chem. Mater*. **1996**, *8*, 2539. Jen, A. K.-Y.; Liu, Y.; Zheng, L.; Liu, S.; Drost, K. J.; Zhang, Y.; Dalton, L. R. *Adv. Mater*. **1999**, *11*, 452.

(7) Rao, V. P.; Jen, A. K.-Y.; Wong, K. Y.; Drost, K. J. *Tetrahedron Lett*. **1993**, *34*, 1747. Rao, V. P.; Cai, C.; Liakatas, I.; Wong, M.-S.; Bösch, M.; Bosshard, C.; Günter, P.; Concilio, S.; Tirelli, N.; Suter, U. W. *Org. Lett*. **1999**, *1*, 1847.

(8) Marder, S. R.; Perry, J. W.; Bourhill, G.; Gorman, C. B.; Tiemann, B. G.; Mansour, K. *Science* **1993**, *261*, 186. Marder, S. R.; Gorman, C. B.; Meyers, F.; Perry, J. W.; Bourhill, G.; Brédas, J.-L.; Pierce, B. M. *Science* **1994**, *265*, 632.

(9) Barzoukas, M.; Blanchard-Desce, M.; Josse, D.; Lehn, J.-M.; Zyss, J. *Chem. Phys*. **1989**, *133*, 323. Slama-Schowk, A.; Blanchard-Desce, M.; Lehn, J.-M. *J. Phys. Chem*. **1990**, *94*, 3894. Blanchard-Desce, M.; Wortmann, R.; Lebus, S.; Lehn, J.-M.; Krämer, P. *Chem. Phys. Lett*. **1995**, *243*, 526. Blanchard-Desce, M.; Runser, C.; Fort, A.; Barzoukas, M.; Lehn, J.-M.; Bloy, V.; Alain, V. *Chem. Phys*. **1995**, *199*, 253. Verbiest, T.; Houbrechts, S.; Kauranen, M.; Clays, K.; Peersons, A. *J. Mater. Chem*. **1997**, *7*, 215. Kim, O.-K.; Fort, A.; Barzoukas, M.; Blanchard-Desce, M.; Lehn, J.-M. *J. Mater. Chem*. **1999**, *9*, 2227.

(10) Wuerthner, F.; Effenberger, F.; Wortmann, R.; Krämer, P. *Chem. Phys*. **1993**, *173*, 305. Steybe, F.; Effenberger, F.; Gubler, U.; Bosshard, C.; Günter, P. *Tetrahedron* **1998**, *54*, 8469.

(11) Cabrera, I.; Althoff, O.; Man, H.-T.; Yoon, H. N. *Adv. Mater*. **1994**, *6*, 43.

(12) Marder, S. R.; Perry, J. W.; Tiemann, B. G.; Gorman, C. G.; Gilmour, S.; Biddle, S. L.; Bourhill, G. *J. Am. Chem. Soc*. **1993**, *115*, 2524.

(13) Blanchard-Desce, M.; Alain, V.; Bedworth, P. V.; Marder, S. R.; Fort, A.; Runser, C.; Barzoukas, M.; Lebus, S.; Wortmann, R. *Chem. Eur. J*. **1997**, *3*, 1091.

(14) Rao, V. P.; Jen, A. K.-Y.; Cai, Y. *J. Chem. Soc., Chem. Commun*. **1996**, 1237. Wong, K. Y.; Jen, A. K.-Y.; Rao, V. P.; Drost, K.; Minnini, R. M.; *Proc. SPIE* **1992**, 74. Jen, A. K.-Y.; Cai, Y.; Bedworth, P. V.; Marder, S. R. *Adv. Mater*. **1997**, *9*, 132.

(15) Cheng, L.-T.; Tam, W.; Marder, S. R.; Stiegman, A. E.; Rikhen, G.; Spangler, C. W. *J. Phys. Chem*. **1991**, *95*, 10643.

(16) Ledoux, I.; Zyss, J.; Jutand, A.; Amatore, C. *Chem. Phys*. **1991**, *150*, 117.

(17) Gilmore, S.; Marder, S. R.; Perry, J. W.; Cheng, L.-T.; *Adv. Mater*. **1994**, *6*, 494.

(18) Rao, V. P.; Wong, K. Y.; Jen, A. K.-J.; Drost, K. J. *Chem. Mater*. **1994**, *6*, 2210.

(19) Inoue, S.; Mikami, S.; Aso, Y.; Otsubo, T.; Wada, T.; Sasabe, H. *Synth. Met*. **1997**, *84*, 395.

(20) (a) Casado, J.; Miller, L. L.; Mann, K. R.; Pappenfus, T. M.; Higuchi, H.; Ortí, E.; Milián, B.; Pou-Amérigo, R.; Hernández, V.; López Navarrete, J. T. *J. Am. Chem. Soc*. **2002**, *124*, 12380. (b) Hernández, V.; Calvo Losada, S.; Casado, J.; Higuchi, H.; López Navarrete, J. T. *J. Phys. Chem. A* **2000**, *104*, 661.

(21) Sakamoto, A.; Furukawa, Y.; Tasumi, M. *J. Phys. Chem*. **1994**, *98*, 4635. Yokonuma, N.; Furukawa, Y.; Tasumi, M.; Kuroda, M.; Nakayama, M. *Chem. Phys. Lett*. **1996**, *255*, 431.

(22) Casado, J.; Hernández, V.; Hotta, S.; López Navarrete, J. T. *J. Chem. Phys*. **1998**, *109*, 10419. Moreno Castro, C.; Ruiz Delgado, M. C.; Hernández, V.; Hotta, S.; Casado, J.; López Navarrete, J. T. *J. Chem. Phys*. **2002**, *116*, 10419. Moreno Castro, C.; Ruiz Delgado, M. C.; Hernández, V.; Shirota, Y.; Casado, J.; López Navarrete, J. T. *J. Phys. Chem. B* **2002**, *106*, 7163.

(23) Casado, J.; Otero, T. F.; Hotta, S.; Hernández, V.; Ramírez, F. J.; López Navarrete, J. T. *Opt. Mater*. **1998**, *9*, 82. Casado, J.; Hernández, V.; Hotta, S.; López Navarrete, J. T. *Adv. Mater*. **1998**, *10*, 1258.

(24) Hernández, V.; Casado, J.; Effenberger, F.; López Navarrete, J. T. *J. Chem. Phys*. **2000**, *112*, 5105. González, M.; Segura, J. L.; Seoane, C.; Martín, N.; Garín, J.; Orduna, J.; Alcala, R.; Villacampa, B.; Hernández, V.; López Navarrete, J. T. *J. Org. Chem*. **2001**, *66*, 8872. Ruiz Delgado, M. C.; Hernández, V.; Casado, J.; López Navarrete, J. T.; Raimundo, J.-M.; Blanchard, P.; Roncali, J. *Chem. Eur. J*. (in press).

(25) Zerbi, G.; Castiglioni, C.; Del Zoppo, M. *Electronic Materials: The Oligomer Approach*; Wiley-VCH: Weinheim, Germany, 1998. Castiglioni, C.; Gussoni, M.; López Navarrete, J. T.; Zerbi, G. *Solid State Commun*. **1988**, *65*, 625. López Navarrete, J. T.; Zerbi, G. *J. Chem. Phys*. **1991**, *94*, 957 and 965. Hernández, V.; Castiglioni, C.; Del Zoppo, M.; Zerbi, G. *Phys. Rev. B* **1994**, *50*, 9815. Agosti, E.; Rivola, M.; Hernández, V.; Del Zoppo, M.; Zerbi, G. *Synth. Met*. **1999**, *100*, 101.

(26) Wiberg, K. B.; Stratmann, R. E.; Frisch, J. M. *Chem. Phys. Lett*. **1998**, *297*, 60. Stratmann, R. E.; Scuseria, G. E.; Frisch, J. M. *J. Chem. Phys*. **1999**, *109*, 8218. Hirata, S.; Lee, T. J.; Head-Gordon, M. *J. Chem. Phys*. **1999**, *111*, 8904. Nguyen, K. A.; Day, P. N.; Pachter, R. *J. Phys. Chem. A* **2000**, *117*, 4748. Hsu, C.-P.; Hirata, S.; Head-Gordon, M. *J. Phys. Chem. A* **2001**, *105*, 451. Nguyen, K. A.; Kennel, J.; Pachter, R. *J. Chem. Phys*. **2002**, *117*, 7128.

(27) Casado, J.; Miller, L. L.; Mann, K. R.; Pappenfus, T. M.; Kanemitsu, Y.; Ortí, E.; Viruela, P. M.; Pou-Amérigo, R.; Hernández, V.; López Navarrete, J. T. *J. Phys. Chem. B* **2002**, *106*, 3872.

(28) Stephens, P. J.; Devlin, F. J.; Chabalowski, C. F.; Frisch, J. M. *J. Phys. Chem*. **1994**, *98*, 11623.

(29) Scott, A. P.; Radom, L. *J. Phys. Chem*. **1996**, *100*, 16502.

(30) Frisch, M. J.; Trucks, G. W.; Schlegel, H. B.; Scuseria, G. E.; Robb, M. A.; Cheeseman, J. R.; Zakrzewski, V. G.; Montgomery, J. A., Jr.; Stratmann, R. E.; Burant, J. C.; Dapprich, S.; Millam, J. M.; Daniels, A. D.; Kudin, K. N.; Strain, M. C.; Farkas, O.; Tomasi, J.; Barone, V.; Cossi, M.; Cammi, R.; Mennucci, B.; Pomelli, C.; Adamo, C.; Clifford, S.; Ochterski, J.; Petersson, G. A.; Ayala, P. Y.; Cui, Q.; Morokuma, K.; Malick, D. K.; Rabuck, A. D.; Raghavachari, K.; Foresman, J. B.; Cioslowski, J.; Ortiz, J. V.; Stefanov, B. B.; Liu, G.; Liashenko, A.; Piskorz, P.; Komaromi, I.; Gomperts, R.; Martin, R. L.; Fox, D. J.; Keith, T.; Al-Laham, M. A.; Peng, C. Y.; Nanayakkara, A.; Gonzalez, C.; Challacombe, M.; Gill, P. M. W.; Johnson, B. G.; Chen, W.; Wong, M. W.; Andres, J. L.; Head-Gordon, M.; Replogle, E. S.; Pople, J. A. *Gaussian 98*, revision A.7; Gaussian, Inc.: Pittsburgh, PA, 1998.

(31) Becke, A. D. *J. Chem. Phys.* **1993**, *98*, 1372.

(32) Novoa, J. J.; Sosa, C. *J. Phys. Chem*. **1995**, *99*, 15837. Raghavachari, K. *Theor. Chem. Acc*. **2000**, *103*, 361.

(33) Rauhut, G.; Pulay, P. *J. Phys. Chem.* **1995**, *99*, 3093.

(34) Pietro, W. J.; Francl, M. M.; Hehre, W. J.; Defrees, D. J.; Pople, J. A.; Binkley, J. S. *J. Am. Chem. Soc.* **1982**, *104*, 5039. Francl, M. M.; Pietro, W. J.; Hehre, W. J.; Binkley, J. S.; Gordon, M. S.; Defrees, D. J.; Pople, J. A. *J. Chem. Phys.* **1982**, *77*, 3654.

(35) Frisch, M. J.; Pople, J. A.; Binkley, J. S. *J. Chem. Phys*. **1984**, *80*, 3265. Clark, T.; Chandrasekhar, J.; Spitznagel, G. W.; Schleyer, P. v. R. *J. Comput. Chem*. **1983**, *4*, 294. Gordon, M. S.; Binkley, J. S.; Pople, J. A.; Pietro, W. J.; Hehre, W. J. *J. Am. Chem. Soc.* **1982**, *104*, 2797.

(36) Woon, D. E.; Dunning, T. H., Jr. *J. Chem. Phys.* **1993**, *98*, 1358. Kendall, R. A.; Dunning, T. H., Jr.; Harrison, R. J. *J. Chem. Phys.* **1992**, *96*, 6796.

(37) Runge, E.; Gross, E. K. U. *Phys. Rev. Lett*. **1984**, *52*, 997. Gross, E. K. U.; Kohn, W. *Adv. Quantum Chem*. **1990**, *21*, 255. Gross, E. K. U.; Ullrich, C. A.; Gossman, U. J. In *Density Functional Theory*; Gross, E. K. U., Driezler, R. M., Eds.; Plenum Press: New York, 1995; p 149.

(38) Casida, M. E. *Recent Advances in Density Functional Methods, Part I*; Chong, D. P., Ed.; World Scientific: Singapore, 1995; p 115.

(39) Koch, W.; Holthausen, M. C. *A Chemist's Guide to Density Functional Theory*; Wiley-VCH: Weinheim, Germany, 2000.

(40) Hutchison, G. R.; Ratner, M. A.; Marks, T. J. *J. Phys. Chem. A* **2002**, *106*, 10596.

(41) Casado, J.; Pappenfus, T. M.; Miller, L. L.; Mann, K. R.; Ortí, E.; Viruela, P. M.; Pou-Amérigo, R.; Hernández, V.; López Navarrete, J. T. *J. Am. Chem. Soc.* **2003**, *125*, 2524.

(42) Clemente, D. A.; Marzotto, A. *J. Mater. Chem.* **1996**, *6*, 941.

(43) The value of *d* is calculated as the average of the lengths calculated for the two C−S bonds adjacent to the exocyclic C═C bond.

(44) Miertus, S.; Scrocco, E.; Tomasi, J. *Chem. Phys.* **1981**, *55*, 117. Cossi, M.; Barone, V.; Cammi, R.; Tomasi, J. *Chem. Phys. Lett*. **1996**, *255*, 327. Amovilli, C.; Barone, V.; Cammi, R.; Cancès, E.; Cossi, M.; Menucci, B.; Pomelli, C. S.; Tomasi, J. *Adv. Quantum Chem.* **1998**, *32*, 227.

(45) Takenaka, T. *Spectrochim. Acta, A* **1971**, *27*, 1735. Girlando, A.; Pecile, C. *Spectrochim. Acta, A* **1973**, *29*, 1859. Faulques, E.; Leblanc, A.; Molini, P.; Decoster, M.; Conan, F.; Guerchais, J. E.; Sala-Pala, J. *Spectrochim. Acta, A* **1995**, *51*, 805.

(46) Khatkale, M. S.; Devlin, J. P. *J. Chem. Phys*. **1979**, *70*, 1851.

(47) Yui, K.; Aso, Y.; Otsubo, T.; Ogura, F. *Bull. Chem. Soc. Jpn.* **1989**, *62*, 1539.

(48) Polivka, T.; Zigmantas, D.; Frank. H. A.; Bautista, J. A.; Herek, J. L.; Koyama, Y.; Fujii, R.; Sundström, V. *J. Phys. Chem. B* **2001**, *105*, 1072.

(49) Negri, F.; Orlando, G.; Zerbetto, F.; Zgierski, M. *J. Chem. Phys.* **1989**, *91*, 6215.

(50) Siebert, T.; Schmitt, M.; Engel, V.; Materny, A.; Kiefer, W. *J. Am. Chem. Soc.* **2002**, *124*, 6242.

(51) Viruela, P. M.; Viruela, R.; Ortí, E.; Brédas, J.-L. *J. Am. Chem. Soc.* **1997**, *119*, 1360. Liu, R.; Zhou, X.; Kasmai, H. *Spectrochim. Acta A* **1997**, *53*, 1241. Altmann, J. A.; Handy, N. C.; Ingamells, V. E. *Mol. Phys.* **1997**, *92*, 339.

(52) van Pham, C.; Burkhardt, A.; Shababa, R.; Cunningham, D. D.; Mark, H. B.; Zimmer, H. *Phosph. Sulf. Silic.* **1989**, *46*, 153.

(53) Chadwick, J. E.; Kohler, B. E. *J. Phys. Chem.* **1994**, *98*, 3631.

(54) Pou-Amérigo, R.; Viruela, P. M.; Viruela, R.; Rubio, M.; Ortí, E. *Chem. Phys. Lett.* **2002**, *352*, 491.

(55) Fabian, J. *Theor. Chem. Acc.* **2001**, *106*, 199.

(56) Jamorski, C.; Foresman, J. B.; Thilgen, C.; Lüthi, H. P. *J. Chem. Phys.* **2002**, *116*, 8761.